Velocity Map Ion Imaging of Chlorine Azide Photolysis: Evidence for Photolytic Production of Cyclic-N₃†

N. Hansen and A. M. Wodtke*

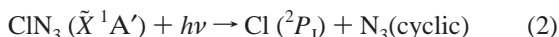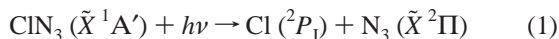*Department of Chemistry and Biochemistry, University of California at Santa Barbara, Santa Barbara, California 93106*

Received: March 13, 2003

The method of velocity map imaging was applied to study the photodissociation dynamics of ClN_3 near 235 nm under collision-free conditions. Derived kinetic energy distributions of state-selected Cl (^2P_J) provide a medium-resolution energy spectrum of the N_3 fragment. Markedly bimodal distributions are observed that suggest simultaneous formation of the linear-N_3 ($\tilde{X}\,^2\Pi$) isomer as well as an energetic form of N_3, consistent with recent theoretical predictions of a cyclic isomer, resembling an isosceles triangle. Angular distributions of the photofragments indicate that $2^1A' \leftarrow 1^1A'$ excitation is the most important pathway to photoproducts. Branching ratio measurements between the dominant spin−orbit excited-state Cl* ($^2P_{1/2}$) and the spin−orbit ground-state Cl ($^2P_{3/2}$) showed Cl*/Cl $\approx 0.8/0.2$. The branching ratio between linear-N_3 and cyclic-N_3 formation was determined to be $\approx 0.8/0.2$.
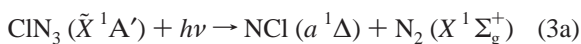
Introduction

Recent interest in the photochemistry of chlorine azide (ClN_3) derives from demonstrations that the primary photoproduct NCl ($a\,^1\Delta$) can be used as an effective energy carrier in chemical iodine lasers.[1−3] Therefore, the photolysis of ClN_3 by near-UV radiation has been examined by Coombe and co-workers,[4−8] Henshaw et al.,[9] and Komissarov et al.[10,11] In these studies, photodissociation was accomplished using pulsed excimer lasers operating at 248 and 193 nm. Unfortunately, the present understanding of the primary photochemical dynamics of chlorine azide is still incomplete.

The UV photochemistry of ClN_3 is quite rich. Several dissociation pathways are possible. Reactions 1 and 2 cleave the N−Cl bond:

$$ClN_3\,(\tilde{X}\,^1A') + h\nu \rightarrow Cl\,(^2P_J) + N_3\,(\tilde{X}\,^2\Pi) \qquad (1)$$

$$ClN_3\,(\tilde{X}\,^1A') + h\nu \rightarrow Cl\,(^2P_J) + N_3(\text{cyclic}) \qquad (2)$$

Reaction 1 forms the linear-azide radical. Recent theoretical calculations suggest that ClN_3 photolysis could form a doublet-state cyclic-N_3 structure that resembles an isosceles triangle.[12]
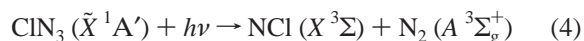
Reaction 3a

$$ClN_3\,(\tilde{X}\,^1A') + h\nu \rightarrow NCl\,(a\,^1\Delta) + N_2\,(X\,^1\Sigma_g^+) \qquad (3a)$$

is believed to be the dominant channel, and also possible is a spin forbidden analogue (reaction 3b):

$$ClN_3\,(\tilde{X}\,^1A') + h\nu \rightarrow NCl\,(X\,^3\Sigma) + N_2\,(X\,^1\Sigma_g^+) \qquad (3b)$$
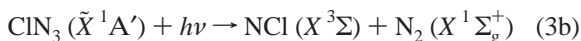
Production of NCl ($X\,^3\Sigma$) is also possible via the spin-allowed channel (reaction 4):

$$ClN_3\,(\tilde{X}\,^1A') + h\nu \rightarrow NCl\,(X\,^3\Sigma) + N_2\,(A\,^3\Sigma_g^+) \qquad (4)$$

N_2 ($A\,^3\Sigma_g^+$), presumably from channel 4, has been detected,[5,6] along with NCl ($b\,^1\Sigma^+$) which can be produced by a second spin-allowed channel (reaction 5):[5,13]

$$ClN_3\,(\tilde{X}\,^1A') + h\nu \rightarrow NCl\,(b\,^1\Sigma^+) + N_2\,(X\,^1\Sigma_g^+) \qquad (5)$$
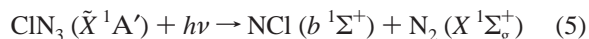
Coombe et al.[6] reported that formation of NCl ($b\,^1\Sigma^+$) and N_2 ($A\,^3\Sigma_g^+$) amount to only $\approx 1\%$ of the 193 nm photolysis products. Komissarov et al.[11] examined the prompt and delayed production of NCl ($A\,^3\Sigma$) using absorption spectroscopy after ClN_3 photolysis at $\lambda = 248$ nm. They estimated that 80% of the primary NCl was formed in the $a\,^1\Delta$ state and, apart from the 1% of NCl ($b\,^1\Sigma^+$), the remaining NCl was thought to be produced in the electronic ground state. Similar measurements for 193-nm photolysis indicated production of $\approx 70\%$ NCl ($a\,^1\Delta$) with 30% NCl ($X\,^3\Sigma$).[10]

Until now, the importance of the atomic channels 1 and 2 has been unknown. Heaven et al.[14] looked at the IR emission produced by 193 nm photolysis of ClN_3. They observed one moderately strong band which was assigned to the N_3 asymmetric stretch. They estimated that the branching fraction leading to Cl-atom production at 193 nm is of the order of 5−10%.

Recently, two additional papers on the velocity map imaging[15] of ClN_3 photoproducts have appeared, from which valuable thermodynamic data was derived. Reaction 6,

$$ClN_3\,(\tilde{X}\,^1A') + 2h\nu \rightarrow ClN_3^+ + e^- \rightarrow$$
$$NCl^+ + N_2\,(X\,^1\Sigma_g^+) + e^- \qquad (6)$$
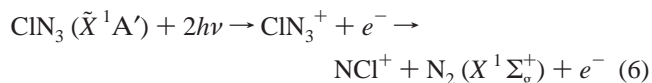
was observed by recording velocity map images of NCl^+ as well as state-selected N_2.[16] In a second paper, the neutral channel 3 above was observed via velocity map images of state-selected N_2.[17] This work provided the most accurate thermochemistry, important to the analysis of reactions 1 and 2 in this work. They derived exoergicities of $\Delta E = +0.21(8)$ eV and $-0.93(9)$ eV
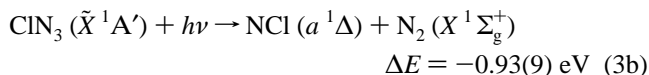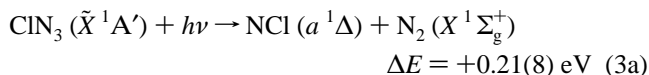
† Part of the special issue "Charles S. Parmenter Festschrift".
* Corresponding author. Phone: 1-805-893-8085. Fax: 1-805-893-4120. E-mail: wodtke@chem.ucsb.edu.

Velocity Map Ion Imaging of ClN$_3$ Photolysis

J. Phys. Chem. A, Vol. 107, No. 49, 2003 **10609**
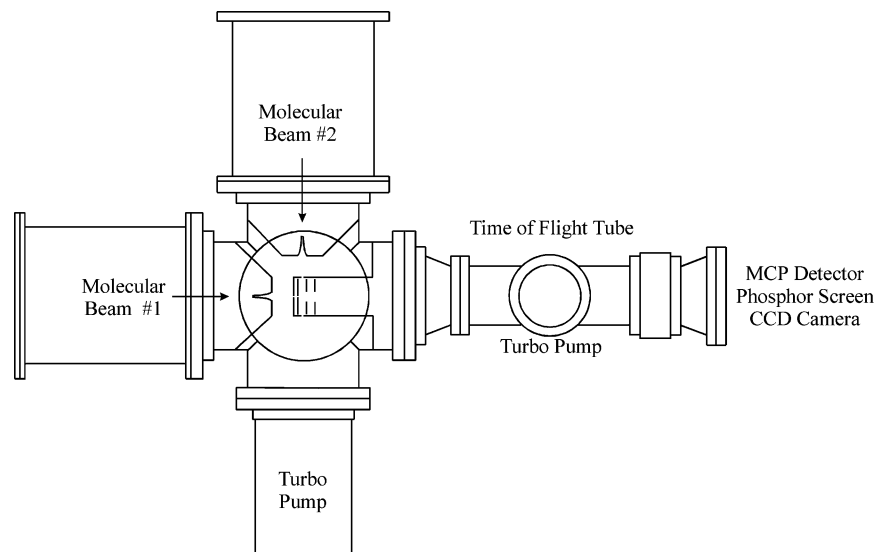
Figure 1. Schematic top view of the velocity map imaging machine. Two molecular beam sources, fixed at 90°, are attached to the six-way 12-in. conflat cross main chamber. The molecular beams cross at the center of the main chamber on the axis of a time-of-flight tube between repeller and extractor of the ion optics. The products are ionized by REMPI using UV lasers typically introduced via smaller ports on top of the machine. Product ions are accelerated by repeller and extractor fields into a 1-m flight tube and strike the position-sensitive detector.

for decomposition of ClN$_3$ into N$_2$ ($X\ ^1\Sigma_g^+$) and NCl ($a\ ^1\Delta$) or NCl ($X\ ^3\Sigma$), respectively:

$$ \text{ClN}_3\ (\tilde{X}\ ^1\text{A}') + h\nu \rightarrow \text{NCl}\ (a\ ^1\Delta) + \text{N}_2\ (X\ ^1\Sigma_g^+) $$
$$ \Delta E = +0.21(8)\ \text{eV} \quad (3\text{a}) $$

$$ \text{ClN}_3\ (\tilde{X}\ ^1\text{A}') + h\nu \rightarrow \text{NCl}\ (a\ ^1\Delta) + \text{N}_2\ (X\ ^1\Sigma_g^+) $$
$$ \Delta E = -0.93(9)\ \text{eV} \quad (3\text{b}) $$

In this work, we report velocity map imaging data for one-photon dissociation of ClN$_3$ near $\lambda \approx 235$ nm, providing another detailed look at the photodissociation dynamics of ClN$_3$ under collision-free conditions. Velocity map images obtained using resonance-enhanced multiphoton ionization (REMPI) of Cl (^2P_J) were bimodal in form and tentatively assigned to dissociation channels 1 and 2. This interpretation implies that the ring structure is located 1.35 ± 0.1 eV above the linear ground electronic state and is therefore the most stable excited state of N$_3$. Branching ratio measurements between the dominant Cl* ($^2P_{1/2}$) and the Cl ($^2P_{3/2}$) showed Cl*/Cl ≈ 0.8/0.2. The angular distributions of the photofragments observed at this wavelength are consistent with initial excitation of the $2^1A' \leftarrow 1^1A'$ absorption system.

Experimental Details

The technique of velocity map imaging has been described fully elsewhere.[15] Here, we provide additional details concerning the apparatus used for these experiments. A schematic of the experiment is shown in Figure 1. The main chamber is a modified six-way 12-in. Conflat cross. Two keying rings have been welded inside, to which the source differential cones are bolted. All components have been manufactured to key together so that there is no adjustment of the molecular beam sources. Each of two source chambers is pumped by high-throughput diffusion pumps. Before entering the main chamber, the molecular beams are collimated ∼2 cm downstream by electro-formed skimmers (Molecular Dynamics). The six-way cross is pumped by a turbo-molecular pump (Osaka Vacuum) to keep the pressure lower than 3×10^{-7} Torr. After passing through one stage of differential pumping and into a separately pumped

time-of-flight chamber, the molecular beams cross in the center of the ion source of a time-of-flight (TOF) mass spectrometer. The products are ionized by REMPI using UV lasers introduced via smaller ports on top of the machine (perpendicular to the plane of Figure 1). Product ions are accelerated by repeller and extractor fields into a 1-m time-of-flight tube. To keep the pressure lower than ∼1×10^{-9} Torr, the region of the ion optics and the time-of-flight tube is pumped by a second turbo-molecular pump (Osaka Vacuum). Product ions strike the position-sensitive detector, which is a 75-mm diameter dual microchannel plate coupled to a phosphor screen (Galileo). Mass-selected images are obtained by pulsing the microchannel plate, typically pulsing from a DC value of −1000 V to −1800 V, with 200 ns duration. A charge-coupled device (CCD) camera (SONY) and a frame grabber (Matrix Vision) are used to download the spatial distribution of the ion signals on the phosphor screen to a computer. Image processing software (LaVision) is used to acquire images. Typically 10 000 laser shots are used to produce the final raw image. The digitized two-dimensional (2D) images are converted to three-dimensional (3D) objects via an inverse Abel transformation using the Basis-Set Expansion method developed by Reisler et al.[18] Velocity and angular distributions are then extracted from the 3D representations.

For these studies, experiments were performed using a single molecular beam source (Molecular Beam #1 in Figure 1) and a single laser providing both dissociation and probe light. ClN$_3$ was formed by passing a mixture of 5% Cl$_2$ in He over the surface of moist sodium azide (NaN$_3$). A standard drying agent was used to remove water from the ClN$_3$/Cl$_2$/He mixture at the exit of the generator. The mixture was then expanded through a pulsed nozzle (General Valve) with a backing pressure of approximately 0.5 bar. No evidence of decomposition of the ClN$_3$ on passage through the pulsed valve was found. Tunable laser light of $\lambda \approx 235$ nm intersected the molecular beam between the repeller plate and the extractor electrode of the ion optics. The laser beam was focused by a 40 cm focal length lens. Laser light near 235 nm was chosen for state-selective ionization of the Cl (^2P_J) products by 2+1 REMPI via the $^2D_{3/2}$ or $^2P_{1/2}$ electronic state for Cl ($^2P_{3/2}$) and Cl* ($^2P_{1/2}$), respectively.[19]
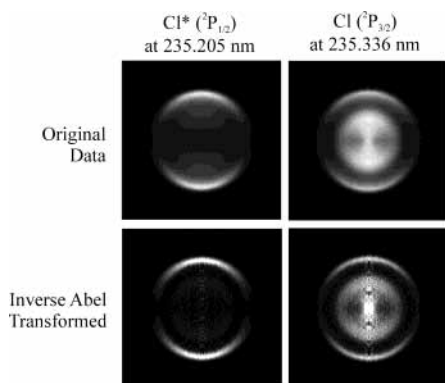
Figure 2. Raw and inverse Abel transformed images of Cl ($^2P_{3/2}$) recorded with dissociation and probe at $\lambda = 235.336$ nm on the $4p$ $^2D_{3/2} \longleftarrow 2p$ $^2P_{3/2}$ transition and of Cl* ($^2P_{1/2}$) recorded with dissociation and probe at $\lambda = 235.205$ nm on the $4p$ $^2P_{1/2} \longleftarrow 2p$ $^2P_{1/2}$ transition. The laser polarization direction is vertical in the plane of the images.

To generate the 235-nm laser light for Cl (^2P_J) atom detection, the doubled output of a Nd:YAG pumped dye laser was mixed with the 1064 nm output of the same Nd:YAG laser. Therefore, ~604 nm light was generated by pumping a pulsed dye laser (Continuum ND 6000 with Rhodamine 610/640 mixture) with the 532-nm output of a seeded Nd:YAG laser (Continuum Powerlite 8000) and subsequently doubled in a KDP crystal. The 302-nm output was then mixed with the 1064 nm IR beam in a second crystal. Approximately $1-2$ mJ/pulse of linearly polarized light was generated in this manner, with a bandwidth of ~ 0.1 cm^{-1}. The laser was scanned back and forth over the Doppler profile of the probed spectral line while the image was acquired.

The velocity space was calibrated by observing the photodissociation of $N_2O \rightarrow N_2$ (X $^1\Sigma_g^+$) + O ($^1D_2$). The N_2 ($v = 0$, $J = 72$) fragment was detected by $2+1$ REMPI via the Q branch of the $a'' X$ $^1\Sigma_g^+ - X$ $^1\Sigma_g^+$ system.[20,21]

Results

These experiments represent one-color studies of the photodissociation of ClN$_3$ at different wavelengths within a narrow range. As such, the photolysis wavelengths change slightly with the specific state probed. Since the absorption spectrum is not discrete in this region,[5] it is assumed that small changes in the available energy do not dramatically influence the dissociation dynamics. The availability of several lines for Cl and Cl* provide a valuable check on this assumption. Both translational energy and angular distributions for the chlorine atom products were insensitive to the particular state probed, confirming that the dynamics do not change rapidly with wavelength in this region.

Chlorine Atom Translational Energy Distribution. Figure 2 shows velocity map images of the Cl$^+$ produced by laser excitation at $\lambda = 235.336$ and 235.205 nm, which probe the Cl ($^2P_{3/2}$) and Cl* ($^2P_{1/2}$), respectively. The upper row shows the original data, while the bottom row shows the result obtained by applying the inverse Abel transformation. These images were taken with the laser vertically polarized, such that the electric vector was parallel to the image plane. Ion intensities in these representations increase from black to white.

An example of the translational energy distribution obtained from the Cl($^2P_{3/2}$) ion image is shown in Figure 3. It is immediately apparent that two mechanisms of dissociation are present, producing "fast" and "slow" Cl atoms. The Cl* ($^2P_{1/2}$) translational energy distribution shows a dominant fast com-
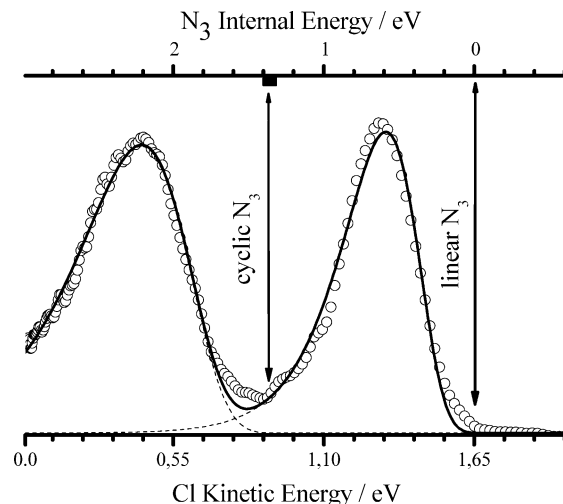
Figure 3. The translational energy distribution for ground-state Cl ($^2P_{3/2}$) derived from the velocity map image shown in Figure 2. The arrow at $E_{kin} = 1.65$ eV marks the maximum possible translational energy to form Cl with linear-N$_3$ ($\tilde{X}$ $^2\Pi$). The double-headed arrow marked "cyclic-N$_3$" shows where a new feature of the Cl atom energy spectrum appears reflecting formation of an excited form of N$_3$. The most recent theoretical predictions of the cyclization energy of N$_3$ are shown as the black bar.
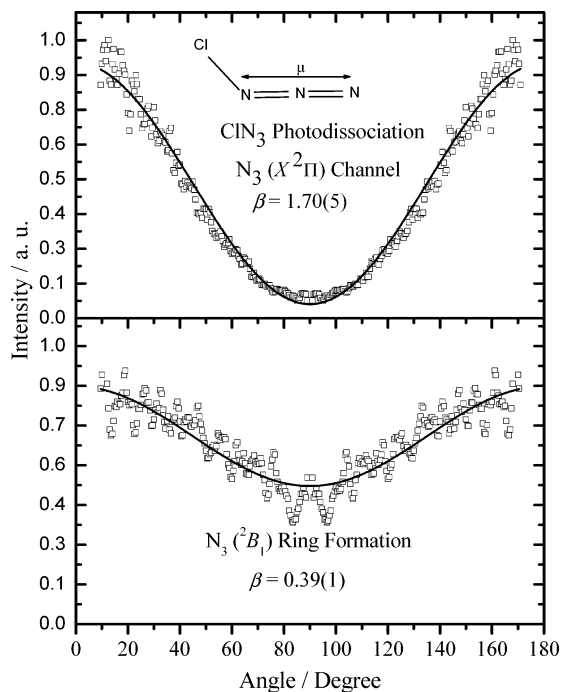
ponent peaking at 1.26 eV and a full width at half-maximum of 0.38 eV. A small contribution (9%) from a "slow" component is also present. In contrast, formation of Cl ($^2P_{3/2}$) ground-state atoms is accompanied by roughly equal amounts (0.56:0.44) of the fast and slow channels, respectively. When ground-state Cl atoms are detected, the fast component peaks at 1.31 eV with a full width at half-maximum of 0.31 eV.

To exclude the possibility that the observed Cl photofragments are produced by photodissociation of Cl$_2$ molecules present in the beam, we performed experiments with a beam of 10% Cl$_2$ in He. Under otherwise identical experimental conditions as the ClN$_3$ experiments we could not observe any Cl fragments. This is undoubtedly due to the very small absorption cross-section of Cl$_2$ at this wavelength.

Chlorine Atom Angular Distributions. From the images of Figure 2, one may clearly see that the "fast channel" shows a substantially more polarized angular distribution than does the "slow channel". This is particularly obvious in the velocity map images of the ground-state Cl-atom. The angular distributions derived from this image are shown in Figure 4 for the "fast" (upper) and "slow" (lower) channels. Fitting the observed angular distribution to the well-known expression $1/4\pi(1 + \beta P_2(\cos \theta))$[22] yields an anisotropy parameter, $\beta = 1.74(4)$, for the "fast" channel. In this expression, θ is the angle between the photofragment recoil vector and the electric field vector of the dissociation laser, $P_2(\cos \theta)$ is the second Legendre polynomial. The value obtained for the "slow" channel is $\beta = 0.41(2)$. The angular distribution for the excited-state chlorine atom is not shown in this work. However, the derived anisotropy parameters are within the error limits the same as for the Cl* atom, in particular, $\beta = 1.70(5)$, for the fast and $\beta = 0.39(1)$ for the slow fragment, respectively.

As will be discussed at length below, the bimodal velocity distributions as well as the clear difference in angular distributions for fast vs slow Cl-atoms is strong evidence that two distinct dissociation mechanisms are taking place when ClN$_3$ is dissociated to N$_3$ radicals and Cl atoms at ~235 nm.

Branching Fractions. The application of REMPI detection of Cl (^2P_J) photofragments to determine the relative spin−orbit

Velocity Map Ion Imaging of ClN$_3$ Photolysis

J. Phys. Chem. A, Vol. 107, No. 49, 2003 **10611**

Figure 4. Chlorine atom Cl ($^2P_{3/2}$) angular distributions obtained from the images in Figure 2. The upper panel shows the observed angular distribution of the "fast" component, the lower panel represents the "slow" component. Squares are experimental points and the lines are the fits yielding $\beta = 1.70(5)$, and $\beta = 0.39(1)$ for the fast and slow components, respectively.

TABLE 1: Branching Ratios of the Cl Photofragments[a]

	Slow	Fast	Total
Cl ($^2P_{3/2}$)	0.1	0.1	0.2
Cl* ($^2P_{1/2}$)	0.1	0.7	0.8
Total	0.2	0.8	1.00

[a] See text for discussion of "fast" and "slow" components.)

branching requires scaling factors to account for the different *n*-photon line-strengths for ionizing Cl ($^2P_{3/2}$) and Cl* ($^2P_{1/2}$), respectively. For each spin−orbit state, the REMPI intensity depends both on the quantum state population and the ionization efficiency. Therefore, scaling factors must be applied to the ratio of REMPI intensities in order to identify the relative spin−orbit branching.

In this work, the relative contributions for the Cl and Cl* were obtained by scaling the integrated REMPI signals using a scaling factor of 0.8(1) for detection of Cl* at 235.205 nm with that for Cl at 235.336 nm.[23] The branching into the different distributions for the Cl and Cl* are summarized in Table 1. In addition to the spin−orbit branching, yielding 79% Cl*, the distributions are further subdivided according to the relative amounts of "fast" and "slow" components. The result gives about four times more fast than slow Cl atom product, with the bulk of the fast Cl appearing as Cl*.

Discussion

Thermodynamic Results. In this section we present newly derived thermodynamic results and review the known thermochemistry of the Cl/N/N/N system, which will be helpful in the analysis that follows. Figure 5 shows the energy levels of ClN$_3$ and related photodissociation products. Here, the N$_3$-producing channels (left side) as well as the N$_2$-producing channels (right side) are shown. All quantities are 0 K heats of formation.

The heat of formation of the N$_3$ ($\tilde{X}\,^2\Pi$) radical was calculated most recently by Martin et al.[24] ($\Delta H_{f,0}^0(N_3) = 4.73$ eV). In
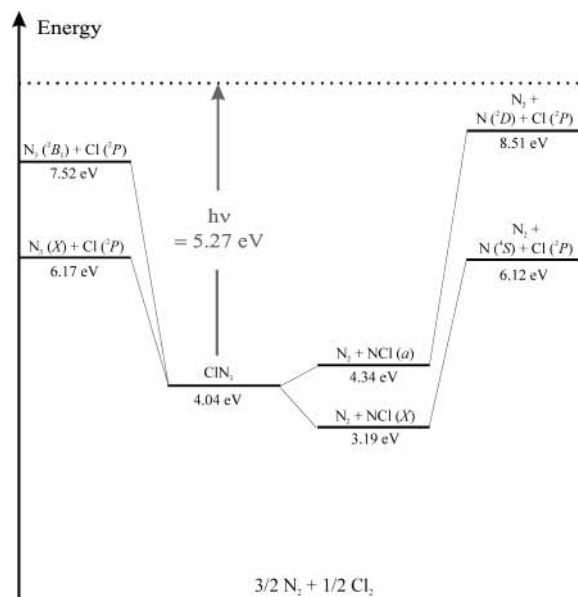

Figure 5. 0 K standard heats of formation (in eV) for molecules that may be constructed from a Cl-atom and three N-atoms.

good agreement with this is the work of Continetti et al.,[25] who determined $\Delta H_{f,0}^0(N_3) = 4.93$ eV, by observing the high-resolution translational energy distributions of the photodissociation products of the N$_3$ molecule. Using the experimental value and the heat of formation of the Cl-atom $\Delta H_{f,0}^0(Cl) = 1.24$ eV) allows us to derive that N$_3$ ($\tilde{X}\,^2\Pi$) + Cl (^2P) lies 6.17 eV above the zero-level. See Figure 5.

Using the heat of formation of N (^4S) and Cl (^2P), we may place N$_2$ ($X\,^1\Sigma_g^+$) + N (^4S) + Cl (^2P) at 6.12 eV. This shows that the linear-N$_3$ ($\tilde{X}\,^2\Pi$) radical is nearly isoenergetic ($D_0 = -0.05$ eV) with respect to the spin-forbidden dissociation to N (^4S) + N$_2$ ($X\,^1\Sigma_g^+$). Using the known excitation energy from N (^4S) to N (^2D) (2.39 eV), we also recognize that the spin-allowed dissociation of linear-N$_3$ ($\tilde{X}\,^2\Pi$) is endoergic by 2.34 eV. This experimentally derived result is in excellent agreement with a recent ab initio calculation (2.37 eV).[12]

We may use the results of the present experiment to gain insight into the values of $D_0(Cl-N_3)$ and with help of the $\Delta H_{f,0}^0(N_3)$ obtain $\Delta H_{f,0}^0(ClN_3)$. The general procedure for the analysis of two-body decay like the one seen here:

$$ClN_3 + h\nu \rightarrow Cl\,(^2P) + N_3 \qquad (1)$$
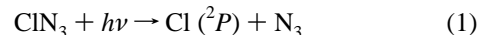
is based on both the evaluation of energy conservation and linear momentum conservation in the center-of-mass frame of the parent molecule. Evaluation of energy conservation can be expressed as shown in eq 7:

$$h\nu - D_0(Cl-N_3) = E_{int}(Cl) + E_T(Cl) + E_{int}(N_3) + E_T(N_3) \qquad (7)$$

where E_{int} represents the internal energies and E_T the translational energies of the fragments, $h\nu$ is the photon energy, and D_0 is the dissociation energy of the parent. Linear momentum conservation can be expressed as shown in eq 8:

$$m_{Cl} E_T(Cl) = m_{N_3} E_T(N_3) \qquad (8)$$

where m_I is the mass of the Ith fragment. Note that use of eqs 7 and 8 allows one to derive the total center of mass release of translation energy from velocity measurements of only one of
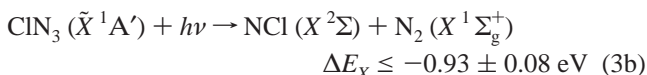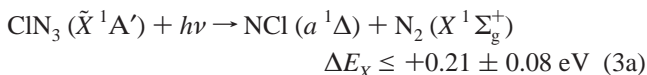
the two fragments. Furthermore, using the velocity map imaging technique allows us to observe the velocities of the Cl-atom fragment by a state-selective method, which yields $E_{int}(Cl)$ and $E_T(Cl)$, leaving $E_{int}(N_3)$ and $E_T(N_3)$ as unknown quantities. These are then unambiguously determined from eqs 7 and 8.

Figure 3 shows the derived translational energy distributions for $Cl(^2P_{3/2})$. We may use this to obtain an upper limit to the dissociation energy of ClN_3, by measurement of the maximum observable translational energy release, $E_T^{MAXlin} = 1.65 \pm 0.1$ eV. To obtain most accurate values for the maximum observable translation energy release, the two components of the translational energy distribution have been fitted to an asymmetric peak function also known in the field of statistics as the Gumbel Minimum Distribution. If we assume that Cl-atoms with this translational energy are formed along with N_3 molecules containing little or no internal excitation, we may use eqs 7 and 8 to obtain $D_0(Cl-N_3) = 2.24 \pm 0.1$ eV. The extent to which the assumption regarding N_3 internal energy is in error lowers the bond energy.

The heat of formation of ClN_3 was first determined experimentally with calorimetric methods by Paillard et al.[26] to be $\Delta H_f^0(ClN_3) = 4.04$ eV. In the same work, those authors determined the HN_3 heat of formation which is in agreement with recent values[27] at the 0.2 eV level of accuracy. This suggests that the calorimetric results for ClN_3 exhibit a similar level of accuracy for ClN_3. Furthermore, Otto and Frenking[28] performed MP2 calculations on the 6-31G(d,p) level of theory-derived $D_0(Cl-N_3) = 2.10$ eV and $\Delta H_f^0(ClN_3) = 4.02$ eV.

In light of the present as well as previous experimental and theoretical work, a consistent picture emerges regarding $D_0(Cl-N_3)$. Using the previously known heats of formation of the chlorine atom, the azide radical, and the parent ClN_3 molecule, we may calculate the dissociation energy $D_0(Cl-N_3) = 2.15 \pm 0.1$ eV. We note that the agreement of the literature bond energy with the present analysis is confirmation that the fastest detected Cl atoms correspond to formation of the linear-azide radical with little or no internal excitation.

In a previous study observing the translational energy release in quantum-state-resolved N_2-photofragments produced by reaction 3, Hansen et al. established rigorous upper limits to the energetics of reactions 3a and 3b:[17]

$$ClN_3 \, (\tilde{X} \, ^1A') + h\nu \rightarrow NCl \, (a \, ^1\Delta) + N_2 \, (X \, ^1\Sigma_g^+)$$
$$\Delta E_X \leq +0.21 \pm 0.08 \text{ eV} \quad (3a)$$

$$ClN_3 \, (\tilde{X} \, ^1A') + h\nu \rightarrow NCl \, (X \, ^2\Sigma) + N_2 \, (X \, ^1\Sigma_g^+)$$
$$\Delta E_X \leq -0.93 \pm 0.08 \text{ eV} \quad (3b)$$

In another velocity map imaging experiment, Hansen et al. observed the translational energy release of NCl^+, produced by reaction 6:

$$ClN_3 \, (\tilde{X} \, ^1A') + 2h\nu \rightarrow ClN_3^+ + e^- \rightarrow$$
$$NCl^+ + N_2 \, (X \, ^1\Sigma_g^+) + e^- \quad (6)$$
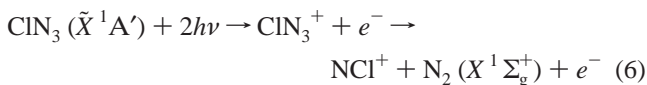
and showed that little or no energy was released as translational energy of the electron.[16] Using published values for the ionization energies of ClN_3[29] as well as NCl,[30] the energetics of reactions 3a and 3b were derived and found to be in excellent agreement with the values presented above. Very recently the energetics of reaction 3a has been calculated at the MRSDCI−CASSCF(12e/10o/D95+d) level of theory and was found to be +0.52 eV.[31]

Using the experimental results and the heat of formation of ClN_3, the heats of formation for NCl can be found: $\Delta H_f^0(NCl \, a \, ^1\Delta) = 4.34 \pm 0.1$ eV and $\Delta H_f^0(NCl \, X \, ^3\Sigma) = 3.19 \pm 0.1$ eV. This may be used to derive the dissociation energies of NCl $(a \, ^1\Delta) \rightarrow N \, (^2D) + N_2 \, (X \, ^1\Sigma_g^+)$ and NCl $(X \, ^3\Sigma) \rightarrow N \, (^4S) + N_2 \, (X \, ^1\Sigma_g^+)$:

$$D_0(N-Cl, a) = 4.17 \pm 0.1 \text{ eV}$$

$$D_0(N-Cl, X) = 2.93 \pm 0.1 \text{ eV}$$

There have been several calculations of $D_0(N-Cl, X)$ which tend to converge from below as the level of theory is improved.[32−37] In the most recent and highest level calculations, Xantheas et al.[37] obtained $D_e = 2.8$ eV, in good agreement with this work.

These new results, and the analysis and the review of past work represent the most definitive exposition of the thermodynamics of the ClN_3 chemical system presently available. All of the recommended thermochemistry is summarized in Figure 5. We believe this picture of the thermochemistry of the Cl/N/N/N system to be accurate to better than 0.1 eV in all cases.

The Primary Photochemical Pathways: Formation of Linear- and Cyclic-N_3. The azide free radical, N_3, has been extensively studied both experimentally and theoretically. The electronic absorption spectrum near 270 nm was first recorded by Thrush[38] and assigned by Douglas and Jones[39] to an $\tilde{A} \, ^2\Sigma_u \leftarrow \tilde{X} \, ^2\Pi_g$ transition of the linear-N_3 molecule. Laser-induced fluorescence (LIF) spectra are also available from Beaman et al.[40] A Fourier transform IR study[41] has shown the ground electronic state to be of $D_{\infty h}$ symmetry with an equilibrium bond length, $R = 1.18115$ Å. Vibrational frequencies of N_3 are available from several experimental studies.[40,42,43] High-quality experimental results revealing the photochemical behavior of the linear-N_3 molecule have also been reported by Continetti et al.[25,44] Calculations of vertical excitation energies of linear-N_3 have been performed at the MRD-CI level by Petrongolo.[45] He predicted the $\tilde{A} \, ^2\Sigma_u$ state to be 4.52 eV above the ground $\tilde{X} \, ^2\Pi_g$ state, in reasonable agreement with the experiment (4.56 eV).[39]

Returning to a consideration of Figure 3, the markedly bimodal translational energy distribution of the Cl-atoms requires explanation. There can be little doubt that the peak at 1.3 eV is due to the formation of the linear ($\tilde{X} \, ^2\Pi$) state of the N_3 radical as this peak extends cleanly to the thermodynamic limit. On the basis of the above-mentioned facts concerning the N_3 radical, it is clear that the Cl-atoms traveling with about 0.5 eV translational energy cannot be due to the production of electronically excited linear-N_3, as the first excited electronic state is energetically out of reach by more than 2 eV. We postulate that the slow channel corresponds to a previously unobserved cyclic isomer of N_3, which lies higher in energy than the linear ground state of N_3. We estimate from the maximum release of Cl-atom translational energy within the slow channel (0.9 ± 0.1 eV−indicated in Figure 3) that the excitation energy of this isomer above the linear ground state is $\Delta E = 1.35 \pm 0.1$ eV.

Although never observed experimentally, nonlinear N_3 isomers have been studied at various levels of theory.[12,46−48] These calculations indicate that a cylic-N_3 isomer with a $^2B_1$ ground state is stable with respect to dissociation or isomerization to the linear form. According to Bittererova et al.,[12] the $^2B_1$ ring structure is the most stable excited state of N_3, located 1.30 eV above the linear ground electronic state at the UHF−CCSD(T) level of theory. The excellent agreement between the theoreti-

cally predicted energetics of the cyclic-N$_3$ and the observed translational energy distributions suggests that the "slow" channel be assigned to the formation of $^2B_1$ N$_3$ cyclic isomer. Recent calculations by the group of Morokuma show the ground state of the cyclic isomer may exhibit $^2A_2$ symmetry. This transition state is nearly isoenergetic with the $^2B_1$ state, and exhibits a different geometry and markedly different bonding. Both states are rings and represent structures relevant to a pseudo rotating triatomic molecule.[31]

This is, to our knowledge, the best experimental evidence for the formation of an all-nitrogen ring molecule.

The energy level of N$_3$ ($^2B_1$) + Cl (^2P) is included in Figure 5. According to theory the N$_3$ ring radical dissociates to the same products as the N$_3$ linear ground electronic state:

$$N_3 \; (^2\Pi, \; ^2B_1) \rightarrow N_2 \; (X\; ^1\Sigma_g^+) + N\; (^2D) \qquad (9)$$
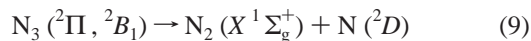
From the experimentally derived energies, a dissociation energy of $D_0(\text{cycl}) = 0.99$ eV can be determined. This is in good agreement with calculations presented by Bitererova et al.[12] At the MR-AQCC computational level, the energy difference between the N$_3$ ($^2B_1$) structure and the dissociation products corrected for ZPE is 1.00 eV. Furthermore, they showed that dissociation of the ring isomer appears to occur over a small barrier (~ 0.3 eV), which is very similar in height to the ring-to-linear isomerization barrier.

Dynamics of the Cl + N$_3$ Channel. We begin a consideration of the photodissociation dynamics with analysis of the angular distributions shown in Figure 4. The angular distribution of Cl-atoms formed with linear-N$_3$ is characterized by an anisotropy parameter $\beta = 1.74$. This is similar to recently measured values of the anisotropy parameter for reactions 3 at 203 nm.

$$ClN_3 \; (\tilde{X}\; ^1A') + h\nu \rightarrow NCl + N_2 \; (X\; ^1\Sigma_g^+)$$
$$\beta = 1.95 \pm 0.06 \qquad (3)$$
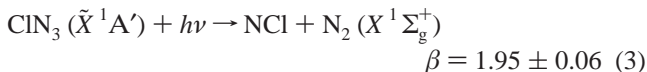
The anisotropy parameter for Cl-atoms formed with cyclic-N$_3$ is $\beta = 0.39$. First of all, it should be clear that the time-scale for dissociation is on the order of a single N−Cl vibrational period for all of these reactions. This suggests that dissociation occurs from a repulsive excited potential surface, an idea consistent with the broad featureless nature of the absorption spectrum.

The absorption spectrum for ClN$_3$ is diffuse but shows a weak absorption, $2\; ^1A' \leftarrow 1^1A'$ peaked near 250 nm with a much stronger absorption system, $2^1A'' \leftarrow 1^1A'$ peaking near 211 nm and another weak absorption $1^1A'' \leftarrow 1^1A'$ near 380 nm.[49] None of the observed angular distributions can be explained by excitation to an A''-state, which would be expected to lead to anisotropy parameters less than zero. Rather it is clear that all of the photochemical products from reactions 1−3 result from initial excitation in the parallel $2^1A' \leftarrow 1^1A'$ system.

Busch and Wilson have shown that the anisotropy parameter may be related to the average angle of departure of the photofragments, α, with respect to the transition dipole moment:[50]

$$\beta = 2 \; P_2(\cos \alpha) \qquad (10)$$

We note that β for reaction 3, formation of N$_2$ + NCl is close to the largest theoretically possible value, $\beta = 2$ and $\alpha = 0°$.[17] This is consistent with the direction of the transition dipole moment nearly parallel to the middle N−N bond in ClN$_3$. See the inset of Figure 4. Considering now reaction 1, forming Cl + linear-N$_3$, we have obtained a value of $\beta = 1.7$. This leads

to a value of $\alpha = 18°$. This is consistent again with photochemistry via the $2^1A' \leftarrow 1^1A'$ absorption system, where the N−Cl bond rupture creates momentum between the Cl and N$_3$ products at a finite angle to the middle N−N bond, consistent with the structure of the ground state. We may also calculate α for the channel where Cl-atoms are formed with cyclic-N$_3$, $\alpha_{\text{cyc}} = 47°$. In contrast, this much larger value suggests substantial structural rearrangement involving dissociation through another transition state. The time scale of dissociation has been recently calculated by Morokuma's group to be less than 25 fs. This time is too short to lead to a broadened angular distribution resulting from parent molecule rotation during dissociation.[31] Nevertheless, since these calculations are still quite preliminary, it cannot be ruled out that cyclic-N$_3$ formation proceeds through a "long-lived" intermediate. For example, a 300 fs lived intermediate would lead to a similar broadening of the angular distribution observed in experiment.

We now consider translational energy distributions of Figure 3. The high-energy peak in Figure 3 lies at $E_T(\text{Cl}) = 1.32$ eV. On the basis of our recommended thermodynamics, we can derive the most probable release of relative translational energy in the center-of-mass frame using eq 8. This leads to $E_T(\text{Cl}) + E_T(\text{N}_3) = 2.45$ eV, which is $\sim 80\%$ of the available energy. This corresponds to a most probable internal energy of the N$_3$ fragment $E_{\text{int}}(\text{N}_3) = 0.74$ eV. We may estimate the N$_3$ rotational excitation, using an impulsive pseudo-triatomic model, where the exit impact parameter is fixed to agree with a value of $\alpha = 18°$. While only an estimate, this analysis suggests that ~ 0.2 eV is channeled to N$_3$ rotation. With this in mind, it appears that linear-N$_3$ is formed with highest probability with ~ 0.5 eV vibrational energy. The translational energy distribution of the Cl* ($^2P_{1/2}$) photofragment looks qualitatively similar. These results are quite similar to results found on the prototypical CH$_3$I photodissociation, where direct dissociation on a repulsive potential governs the dissociation dynamics.[51,52]

In contrast to the formation of linear-N$_3$, the translational energy distribution for cyclic-N$_3$ formation channels a larger fraction ($\sim 50\%$) of the available energy to internal excitation of the N$_3$ fragment. Indeed compared to the linear-N$_3$ forming channel, there is more internal energy (0.95 eV), despite the substantially smaller amount of available energy. We believe that this is further evidence for formation of the cyclic-N$_3$ as the closing of the ring is likely to lead to larger amounts of vibrational excitation.

These experiments do not allow us to investigate a subsequent fate of the cyclic-N$_3$ fragment. Indeed nothing is known about how this molecule might decompose by spontaneous unimolecular processes. Specifically, there is nothing known about the dissociation barrier for the spin-forbidden dissociation channel. However, we can say that the great majority of the cyclic-N$_3$ formed here appear to be at energies less than that required to dissociate in the spin-allowed channel, forming N$_2$ ($X\; ^1\Sigma_g^+$) + N (^2D).[12]
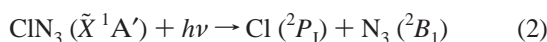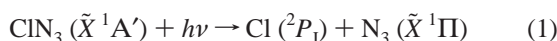
For the slow-moving Cl atoms there are in principle other explanations possible. For instance a bimodal distribution of vibrational energies in the N$_3$ fragment cannot be ruled out. But preliminary theoretical calculations on the first two excited electronic states show that dissociation to form the linear-azide radical occurs on a purely repulsive potential energy surface where one expects a large fraction of the available energy to be channeled to translation.[31] Therefore it seems unlikely that the photodissociation of ClN$_3$ forming linear-azide radical would result in a bimodal vibrational distribution. Furthermore, Figure 5 shows that the three-body dissociation of chlorine azide to

Cl (^2P_J) + N (^4S) + N$_2$ (X $^1\Sigma_g^+$) is energetically equal to the formation of linear-N$_3$ ($\tilde{X}$ $^2\Pi$) + Cl (^2P_J). But it is unlikely that the angular distributions of Cl atoms coming from three-body dissociation would appear as sharply peaked as is observed in this work. And in addition, the three-body dissociation mechanism would be spin-forbidden. Recently, we have observed velocity map ion images of N (^2D) that result from photolysis of the energetic component of the N$_3$ primary photofragments.[53] Should three-body dissociation be the sole explanation of the slow-moving Cl atoms no such N (^2D) signal would be expected.

In summary, both the observed energetics and dynamics, including broader product angular distribution and more internal excitation, support the assignment of the slow channel to cyclic-N$_3$ formation.

Conclusions

We observed 2+1 REMPI signals and ion velocity maps of state-selected Cl (^2P_J), resulting from the one-photon dissociation of ClN$_3$. Two channels were observed and tentatively assigned to:

$$\text{ClN}_3 \, (\tilde{X} \, ^1A') + h\nu \rightarrow \text{Cl} \, (^2P_J) + \text{N}_3 \, (\tilde{X} \, ^1\Pi) \quad (1)$$

$$\text{ClN}_3 \, (\tilde{X} \, ^1A') + h\nu \rightarrow \text{Cl} \, (^2P_J) + \text{N}_3 \, (^2B_1) \quad (2)$$

About 0.70 eV internal energy is deposited in the N$_3$ ($\tilde{X}$ $^2\Pi$) radicals formed in channel 1. The observation of channel 2 is the first experimental evidence of the N$_3$-ring isomer. This state was found to be 1.35 eV above the linear-N$_3$ ground state—in very good agreement with recent calculations. The derived anisotropy parameters of the Cl angular distribution for channels 1 and 2 indicate a parallel transition. Therefore, the $2^1A' \leftarrow 1^1A'$ absorption system is responsible for production of photoproducts at this wavelength.

We also obtained the spin–orbit Cl/Cl* branching ratio ($\approx 0.2/0.8$) in the UV photolysis of ClN$_3$ near 235 nm, and furthermore we obtained the relative importance of channels 1 and 2 to be $\approx 0.8/0.2$ in favor of channel 1.

References and Notes

(1) Ray, A. J.; Coombe, R. D. *J. Phys. Chem.* **1995**, *99*, 7849.
(2) Henshaw, T. L.; Manke, G. C.; Madden, T. J.; Berman, M. R.; Hager, G. D. *Chem. Phys. Lett.* **2000**, *325*, 537.
(3) Manke, G. C.; Hager, G. D. *J. Mod. Opt.* **2002**, *49*, 465.
(4) Ray, A. J.; Coombe, R. D. *J. Phys. Chem.* **1994**, *98*, 8940.
(5) Coombe, R. D.; Patel, D.; Pritt, A. T.; Wodarczyk, F. J. *J. Chem. Phys.* **1981**, *75*, 2177.

(6) Coombe, R. D.; David, S. J.; Henshaw, T. L.; May, D. J. *Chem. Phys. Lett.* **1985**, *120*, 433.
(7) Coombe, R. D.; Vanbenthem, M. H. *J. Chem. Phys.* **1984**, *81*, 2984.
(8) Jensen, R. H.; Mann, A.; Coombe, R. D. *J. Phys. Chem. A* **2000**, *104*, 6573.
(9) Henshaw, T. L.; Herrera, S. D.; Haggquist, G. W.; Schlie, L. A. V. *J. Phys. Chem. A* **1997**, *101*, 4048.
(10) Komissarov, A. V.; Manke, G. C., II; Davis, S. J.; Heaven, M. C. *Proc. SPIE—Int. Soc. Opt. Eng.* **2000**, *3931*, 138.
(11) Komissarov, A. V.; Manke, G. C.; Davis, S. J.; Heaven, M. C. *J. Phys. Chem. A* **2002**, *106*, 8427.
(12) Bittererova, M.; Ostmark, H.; Brinck, T. *J. Chem. Phys.* **2002**, *116*, 9740.
(13) Pritt, A. T.; Patel, D.; Coombe, R. D. *J. Chem. Phys.* **1981**, *75*, 5720.
(14) Heaven, M. C. Private communication.
(15) Eppink, A.; Parker, D. H. *Rev. Sci. Instrum.* **1997**, *68*, 3477.
(16) Hansen, N.; Wodtke, A. M.; Komissarov, A. V.; Morokuma, K.; Heaven, M. C. *J. Chem. Phys.* **2003**, *118*, 10485.
(17) Hansen, N.; Wodtke, A. M.; Komissarov, A. V.; Heaven, M. C. *Chem. Phys. Lett.* **2003**, *268*, 568.
(18) Dribinski, V.; Ossadtchi, A.; Mandelshtam, V. A.; Reisler, H. *Rev. Sci. Instrum.* **2002**, *73*, 2634.
(19) Arepalli, S.; Presser, N.; Robie, D.; Gordon, R. J. *Chem. Phys. Lett.* **1985**, *118*, 88.
(20) Neyer, D. W.; Heck, A. J. R.; Chandler, D. W. *J. Chem. Phys.* **1999**, *110*, 3411.
(21) Rijs, A. M.; Backus, E. H. G.; de Lange, C. A.; Janssen, M. H. M.; Wang, K.; McKoy, V. *J. Chem. Phys.* **2001**, *114*, 9413.
(22) Zare, R. N. *Mol. Photochem.* **1972**, *4*, 1.
(23) Liyanage, R.; Yang, Y. A.; Hashimoto, S.; Gordon, R. J.; Field, R. W. *J. Chem. Phys.* **1995**, *103*, 6811.
(24) Martin, J. M. L.; Francois, J. P.; Gijbels, R. *J. Chem. Phys.* **1990**, *93*, 4485.
(25) Continetti, R. E.; Cyr, D. R.; Osborn, D. L.; Leahy, D. J.; Neumark, D. M. *J. Chem. Phys.* **1993**, *99*, 2616.
(26) Paillard, C.; Moreau, R.; Combouri, J. *C. R. Acad. Sci. C* **1967**, *264*, 1721.
(27) Zhang, J. S.; Xu, K. S.; Amaral, G. *Chem. Phys. Lett.* **1999**, *299*, 285.
(28) Otto, M.; Lotz, S. D.; Frenking, G. *Inorg. Chem.* **1992**, *31*, 3647.
(29) Frost, D. C.; Macdonald, C. B.; McDowell, C. A.; Westwood, N. P. C. *Chem. Phys.* **1980**, *47*, 111.
(30) Butcher, V.; Dyke, J. M.; Lewis, A. E.; Morris, A.; Ridha, A. *J. Chem. Soc.—Faraday Trans. 2* **1988**, *84*, 299.
(31) Morokuma, K. Private communication.
(32) Lievin, J.; Metz, J. Y. *Theor. Chim. Acta* **1985**, *67*, 391.
(33) Peterson, K. A.; Woods, R. C. *J. Chem. Phys.* **1990**, *93*, 1876.
(34) Milburn, R. K.; Rodriquez, C. F.; Hopkinson, A. C. *J. Phys. Chem. B* **1997**, *101*, 1837.
(35) Bettendorff, M.; Peyerimhoff, S. D. *Chem. Phys.* **1986**, *104*, 29.
(36) Papakondylis, A.; Mavridis, A.; Metropoulos, A. *J. Phys. Chem.* **1995**, *99*, 10759.
(37) Xantheas, S. S.; Dunning, T. H.; Mavridis, A. *J. Chem. Phys.* **1997**, *106*, 3280.
(38) Thrush, B. A. *Proc. R. Soc. London Ser. A* **1956**, *235*, 143.
(39) Douglas, A. E.; Jones, W. J. *Can. J. Phys.* **1965**, *43*, 2216.
(40) Beaman, R. A.; Nelson, T.; Richards, D. S.; Setser, D. W. *J. Phys. Chem.* **1987**, *91*, 6090.
(41) Brazier, C. R.; Bernath, P. F.; Burkholder, J. B.; Howard, C. J. *J. Chem. Phys.* **1988**, *89*, 1762.
(42) Tian, R. J.; Facelli, J. C.; Michl, J. *J. Phys. Chem.* **1988**, *92*, 4073.
(43) Pahnke, R.; Ashworth, S. H.; Brown, J. M. *Chem. Phys. Lett.* **1988**, *147*, 179.
(44) Continetti, R. E.; Cyr, D. R.; Metz, R. B.; Neumark, D. M. *Chem. Phys. Lett.* **1991**, *182*, 406.
(45) Petrongolo, C. *J. Mol. Struct.* **1988**, *175*, 215.
(46) Martin, J. M. L.; Francois, J. P.; Gijbels, R. *J. Chem. Phys.* **1989**, *90*, 6469.
(47) Wasilewski, J. *J. Chem. Phys.* **1996**, *105*, 10969.
(48) Klein, R.; Biskupic, S. *Chem. Pap.—Chem. Zvesti* **1993**, *47*, 143.
(49) Dehnicke, K.; Ruschke, P. *Z. Naturforsch. (B)* **1978**, *33*, 750.
(50) Busch, G. E.; Wilson, K. R. *J. Chem. Phys.* **1972**, *56*, 3638.
(51) Sparks, R. K.; Shobatake, K.; Carlson, L. R.; Lee, Y. T. *J. Chem. Phys.* **1981**, *75*, 3838.
(52) Eppink, A.; Parker, D. H. *J. Chem. Phys.* **1999**, *110*, 832.
(53) Hansen, N.; Goncher, S. J.; Wodtke, A. M. Unpublished.